



## Investigation of bio-removing metal ions from wastewater—a viewpoint of micro forces

Huaigang Cheng, Huiping Song\*

*Institute of Resources and Environment Engineering, State Environment Protection Key Laboratory of Efficient Utilization of Coal Waste Resources, Shanxi University, Taiyuan 030006, China, Tel./Fax: +86 351 7018813; email: songhp@sxu.edu.cn (H. Song)*

Received 22 April 2014; Accepted 18 August 2014

### ABSTRACT

Biosorption is one of the effective methods to treat the wastewater containing heavy metal ions, especially the biosorption using magnetotactic biosorbents (MTB). The interaction between metal ions and MTB was investigated using molecular dynamics simulations. A model of a bacterial cell consisting of functional groups and  $\text{Fe}_3\text{O}_4$  was created. The principal functional groups on the MTB surface included  $-\text{COOH}$ ,  $-\text{PO}_3\text{H}_2$ , and  $-\text{OH}$ , and physical adsorption was deduced as the primary adsorption mechanism. Free energy profiles for ions approaching the bacterial cell were computed using the adaptive biasing force method. The adsorption of ions occurred at a distance of 5 Å from the MTB surficial groups. Repulsive force had to be overcome when ions approached the functional groups in the simulation. The electrostatic attraction between ions and the adsorbent promotes adsorption, while the van der Waals force hinders adsorption. The  $-\text{PO}_3\text{H}_2$  and  $-\text{COOH}$  groups were found to contribute to the adsorption selectivity in the binary aqueous solutions.

*Keywords:* Magnetotactic bacterium; Biosorption; Metal Ions; Molecular dynamics simulation

### 1. Introduction

Research on microbial adsorption receives great attention because of its potential applications for wastewater treatment and environmental protection [1,2]. Among the micro-organisms used, magnetotactic bacteria (MTB) have proven to be efficient biosorbents [3,4]. These bacteria contain a magnetosome consisting primarily of  $\text{Fe}_3\text{O}_4$  or  $\text{Fe}_3\text{S}_4$  arranged in chains [5], which enables many applications [6–8] such as fixed enzyme carriers, targeted nanomedicine carriers, magnetic recorders, and recycling agents for removal of metal from wastewater. MTB [3] possess unique magnetotactic properties and ideal adsorption of metal

ions. With the aid of a high-gradient magnetic field [9], metal-loaded MTB can be rapidly removed from wastewater, which bypasses the problem of separating the adsorbed metal ions from the solution through other biosorption processes.

For application of MTB to water treatment, Bahaj [10,11] examined the separation process and found the method to be adequate for removing and recycling heavy metals. This method also permits rapid adsorption and a large adsorption capacity [12]. Many micro-organisms can adsorb metal ions because of their metabolism; however, MTB display a remarkable adsorption preference for heavy metals over other ions. In the adsorption of metal ions, heavy ions such as Au(III), Ag(I), Cu(II), Ni(II), and Pd(II) are adsorbed by MTB with higher selectivity than other ions. The

\*Corresponding author.

adsorption selectivity of coexisting heavy metal ions has also been clearly demonstrated. For example, a large difference was noted for MTB adsorption of Au (III) and Cu(II) [12] mixed in wastewater, although similar adsorption efficiencies were achieved for each of the single-element solutions. For the practical use of MTB in optimizing wastewater treatment, the adsorption mechanism is of great importance. Recent experiments [13,14] have examined the adsorption mechanism of MTB. Because the microscopic phenomenon was not easily observed experimentally, the mechanism of adsorption was often discussed in terms of the adsorption isotherm and fitted to thermodynamic models. However, the adsorption process must be directly observed and explored at the microscopic level. Therefore, this type of theoretical research was performed in the present study.

Much research in the area of adsorption [15,16], including the thermodynamics or kinetics of multi-component systems, is important for the present study. The insights provided by the literatures can be summarized into three research methods: the first is in the field of physical chemistry; these methods involve fitting the adsorption free energy or other physicochemical parameters using experimental data to evaluate the likelihood of adsorption. The second method examines the adsorption mechanism based on the determination of functional groups on adsorbent surfaces using advanced instrumental analysis. The third method is computer simulation at the microscopic level, which has been successfully used to calculate the adsorbent structure, pervasion, and adsorbent–adsorbate interaction or other interactions [17–19].

Previous studies largely focused on the physical and chemical properties of the micro-organism itself when examining its biosorption. However, the mechanism by which ions are captured from their free status in aqueous solution and bound to the adsorption sites of MTB as well as the effect of each of the MTB surficial groups on the adsorption of ions remain unclear. MTB are a polyphyletic group of bacteria, including rod-shaped, curved, spherical, and helical bacteria of various dimensions and structure. Many differences exist in the abilities of the functional groups to capture adsorbates. All ions do not share the same affinity for certain groups. Thus, the following questions must be addressed: What functional groups exist on the MTB surface? What roles do these groups play in the adsorption of ions and how does the interaction between the groups and the ions affect the adsorption selectivity? Microscopically, different types of interactions can affect the diffusion and adsorption, such as van der Waals and electrostatic forces, hydrogen bonding, conformational entropy. Sufficiently accurate

measurements [20,21] of the interactions between the ions and the bacterial surface groups, as well as the probability distribution of the ion displacement trajectories, would be helpful in analyzing the adsorption tendency and furthering our understanding of adsorption. Therefore, the molecular characterization of microscopic interactions can be considered as an essential step for the optimization of adsorption process for environmental and industrial applications.

It is well known that the adsorption can be affected by the macroscopic operation conditions such as pH value and ionic strength. One of the reasons is that the micro-intermolecular forces are changed with the changes in the charge distribution of the system. Ionic interactions is commonly one of the most important forces driving adsorbate approach to adsorbent, which depend on the details of the charge or micro-structure of groups of the adsorbent and the given adsorbate involved. However, it is difficult to assess the contribution of the ionic interactions at the microscopic level. The atomic force microscope system is undoubtedly one of the best tools for direct measurements of micro-structural parameters and intermolecular forces with atomic-resolution characterization [22], but difficulties still exist in the direct observation of the interaction between free ions and adsorbent surfaces. For such a micro-scale study, molecular simulation can certainly provide a characterization of different interactions in the adsorption process. For the effect of non-bonded interaction on the structural features of molecules and ions, many methods such as the *ab initio* calculation were applied successfully [23]. For the study of dynamic characteristics of interfacial system, molecular dynamics simulation is considered to be preferable. Some simulations of the conformational and adsorption properties of organic adsorbents have been performed recently and insights into the organic molecular immobilization and the substrate diffusion through pores were provided for instance [24]. It was found that the electrostatic interactions were responsible for the interfacial adhesion, but van der Waals forces were detrimental. The role of micro-level interactions can also be studied by other simulation methods such as truncated electrostatic calculation [25], switching on/off micro-forces [26], dissipative particle dynamics [27], etc. which are ideal tools to provide information that cannot be investigated experimentally.

This study evaluated the adsorption of aqueous heavy metal ion onto magnetotactic bacteria at the microscopic level. For this purpose, the bacteria will be considered as a combination of functional groups, and adsorption will be treated as a process of ion approach to the bacteria.

## 2. Experimental and simulation method

### 2.1. Experimental details

The surface groups cause the MTB to capture the metal ions. In this study, Fourier transform infrared spectroscopy (Nexus, Thermo, USA) was used to detect these chemical groups. The species and the density of the bacterial surface groups were then further determined via potentiometric titration [28] using a 2.5 g/l biomass. A 0.25 g wet biomass was suspended in 100 ml of deionized water, and NaOH or HNO<sub>3</sub> solutions were added to maintain a pH of 2. The suspension was agitated in a N<sub>2</sub> atmosphere at room temperature for 24 h. A standard NaOH solution (0.1 mol/l) was used to titrate the suspension until the pH reached 13, as detected by a pH meter. The N<sub>2</sub> atmosphere was maintained during the titration.

A surface complexation model [28] was chosen to process the data from the potentiometric titration. The logarithm of the dissociation constants ( $pK_a$ ) and the densities ( $N$ ) of the MTB surface groups were obtained using regression analyses [29]. Each functional group had its own specific  $pK_a$  value. Therefore, based on the  $pK_a$  values in the literature, the groups existing on the MTB surface were deduced.

To verify the existence of the deduced groups, a chemical modification was applied to the MTB to block some of the functional groups. Methanol and hydrochloric acid were used to block –COOH, formic acid was used to block –OH, and triethyl phosphite and nitromethane were used to block –PO<sub>3</sub>H<sub>2</sub>, respectively. The chemical modification method blocked certain chemical groups on the adsorbent, and the performance of the MTB was compared with that of the original adsorbent using adsorption tests that reflected the role of the functional group.

### 2.2. Simulation method

Molecular dynamics simulation was used to investigate the adsorption process from the perspective of ion diffusion and free energy change under the influence of the MTB surface groups. The NAMD simulation package with the CHARMM force field was used for the molecular dynamics simulation. The NAMD simulation [30,31] was developed by the theoretical and computational biophysics group at the Beckman Institute for Advanced Science and Technology at the University of Illinois at Urbana-Champaign. The CHARMM force field was developed to simulate proteins and lipids. The CHARMM force field has also been successfully utilized to simulate the dynamic behavior of inorganic molecules, e.g. the moving dynamics of water droplets on a solid surface with

respect to the microscopic motions of water molecules [32]. This force field has also been applied to simulate some of the metals [33–35] and metals bound with proteins [36].

In this simulation, an MTB molecule representing an adsorption site on a bacterium was represented by a solid magnetosome (Fe<sub>3</sub>O<sub>4</sub>) ball grafted with the functional groups. The Fe<sub>3</sub>O<sub>4</sub> ball was considered to be a spherical segment of the lattice-like magnetite [37,38]. The metal ions were represented as the form of free residues, whose force field parameters were adopted from the literature [39,40]. As is well known, it is difficult to describe heavy metals with classic force fields, because most of the heavy metals are transition metals and the quantum effects cannot be neglected. Therefore, only the non-bonded effects are directly investigated in the simulation. A simplified method was introduced in the literature for the modeling of the interaction between the metal atoms and the functional groups [41]: only the metal atoms close to the functional group were considered in the bonded interactions, whereas the interactions between the group and other surrounding metal atoms were modeled using a Lennard-Jones potential. Because this simulation sought to examine the diffusion of ions, the distance between the ions and the functional group was maintained as more than 5 Å so that the bonded interactions could be ignored.

To highlight the function of a single adsorption site, a water sphere was used rather than a water box. A spherical simulation system containing an MTB molecule, an ion, and 3,821 water molecules was constructed with a diameter of 60 Å as shown in Fig. 2. Counter ions (Cl<sup>–</sup>) were added randomly to neutralize the charge of the system. The number of groups grafted onto the simulated MTB molecule was equal to those on a 100 Å<sup>2</sup> surface of an actual MTB, which indicates that the spherical system actually simulated the aqueous solutions near the 1 nm<sup>2</sup> surface of the MTB. No periodic boundary conditions were applied, and chloride ions were used to balance the charge in the system. The water model used in this study was the transferable intermolecular potential.

The simulation was conducted in the constant temperature, constant pressure ensemble (NPT). The adsorption of ion onto the MTB was not obviously pH sensitive, because the adsorption yield was always greater than 95% when the pH was 2~7 [12], which is the pH range typical of heavy metal loaded wastewater [42,43]. Therefore, the impact of pH was not considered, and neutral conditions were accepted for the simulation. The van der Waals energy was calculated with the standard 12–6 Lennard-Jones potential, and the electrostatic energy was calculated with the

Coulombic potential. In this study, the van der Waals interactions were truncated smoothly using a 12 Å cut-off in conjunction with a switching function at 10 Å. A time step of 2 fs was used for all simulations. Energy minimizations of 20 ps and a relaxation of 4 ns were conducted until the system was equilibrated. The ion trajectories were calculated to aid in understanding their diffusion behavior. The ion diffusion biases and adsorption selectivity were evaluated using the probability distribution of their trajectories at different distances from the MTB molecule. The site of an MTB cell was determined by the average coordinates of its atoms. The distance between the ion and the MTB molecule ( $\zeta$ ) was subsequently calculated based on their coordinates.

An ion would not spontaneously diffuse toward the MTB in the simulation. Thus, a steered molecular dynamics (SMD) simulation was applied to push the ion toward the surface of the MTB molecule. The SMD imitated the basic idea of atomic force microscopy by forcibly pulling a given atom or group along the route specified during the simulation process. Three SMD simulations were conducted with different spring constants of 0.01, 0.1, and 1 kcal/mol/Å<sup>2</sup>, and 0.1 kcal/mol/Å<sup>2</sup> was found to be the most appropriate by comparing the simulation with the experimental results for the free energy change. The movement velocity was fixed at 0.01 Å/ps. Jarzynski's equality was applied to calculate the free energy with respect to the internal coordinates. The potential of mean force was calculated to represent the free energy ( $\Delta G^\circ(\zeta)$ ) profile as a function of the coordinate, which was referred to as the reaction coordinate. Ten different starting points and moving trajectories of the ions were tested, and the average values were calculated to analyze the simulation results.

### 3. Results and discussion

#### 3.1. Structure of the MTB molecule

Fig. 1 and Table 1 present the MTB's infrared spectra before and after the adsorption of the heavy metal ions. No significant differences were observed among the overall spectral shapes, but some of the positions and intensities of the characteristic peaks changed slightly. This phenomenon indicated that the composition and structure of the cells did not change with the adsorption of the metal ions, but surface groups, such as hydroxyl, carboxyl, and phosphonyl groups, were all involved in adsorption. In Table 1, the chemical modifications on the MTB were effective relative to the modifications reported in the literature [44–46].

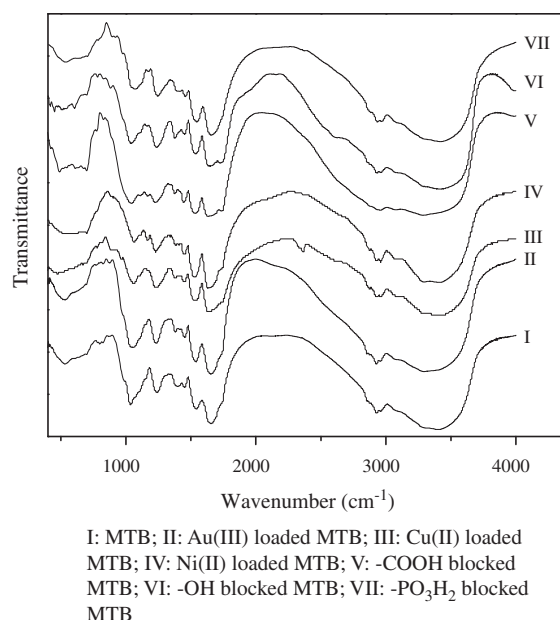


Fig. 1. The infrared spectra of MTB before and after the adsorption of heavy metal ions.

For example, because an acetyl group was introduced during the modification of -OH, a peak at 1,740 cm<sup>-1</sup> was observed indicating the stretching vibration of C=O. The characteristic peaks ranging from 1,300 to 1,050 cm<sup>-1</sup> were also strengthened and their displacements revealed the conversion of a hydroxyl to an ester. The modified MTB was then placed into the aqueous solution for adsorption of Cu(II). The experimental results provided in Table 2 indicate that the bacterial adsorption of Cu(II) was greatly altered by treatment with chemical reagents. Sorting of the modified MTB by decreasing the adsorption ratio shows that the -COOH-blocked MTB lost most of its adsorption capacity, followed by -OH- and -PO<sub>3</sub>H<sub>2</sub>-blocked MTB. This finding indirectly indicates that -COOH may be one of the most important groups in the MTB adsorption process.

The values of  $pK_a$  and  $N$  for the surface groups of the MTB are shown in Table 3, from which a coefficient of determination ( $R^2$ ) of 0.9984 was calculated, thereby indicating that the surface complexation model correctly accounted for the experimental results. According to the literature [47–50], -COOH (  $\begin{matrix} \text{OH} \\ | \\ -\text{C}=\text{O} \end{matrix}$  ), -PO<sub>3</sub>H<sub>2</sub> (  $\begin{matrix} \text{OH} \\ | \\ -\text{P}=\text{O} \\ | \\ \text{OH} \end{matrix}$  ), and -OH were finally identified, which was also in agreement with the literature [51,52].

Table 1  
Characteristic peaks of infrared spectra of the MTB

| Bonds                 | Wave number (cm <sup>-1</sup> ) |                    |                   |                   |                       |                   |  |
|-----------------------|---------------------------------|--------------------|-------------------|-------------------|-----------------------|-------------------|--|
|                       | MTB                             | Au(III)-loaded MTB | Cu(II)-loaded MTB | Ni(II)-loaded MTB | -COOH-blocked MTB     | -OH-blocked MTB   | -PO <sub>3</sub> H <sub>2</sub> -blocked MTB |
| C=O                   | 1,650                           | 1,640              | 1,630             | 1,630             | 1,640                 | 1,740             | 1,650  |
| C=O, N-H              | 1,540                           | 1,520              | 1,520             | 1,530             | 1,530                 | 1,540             | 1,540  |
| C-N, N-H              | 1,240                           | 1,240              | 1,220             | 1,160             | 1,240                 | 1,240             | 1,240  |
| -OH, -NH <sub>2</sub> | 3,380                           | 3,300              | 3,350             | 3,390             | 3,380                 | 3,430<br>(weaken) | 3,380  |
| C-H                   | 1,450                           | 1,450              | 1,440             | 1,450             | 1,450                 | 1,451             | 1,450  |
| -CH <sub>3</sub>      | 2,930                           | 2,930              | 2,930             | 2,930             | 2,930                 | 2,931             | 2,930  |
| -OH, C-O-C            | 1,040                           | 1,050              | 1,050             | 1,060             | 1,040<br>(strengthen) | 1,300~1,050       | 1,040  |
| P=O                   | 1,400                           | 1,380              | 1,370             | 1,380             | 1,400                 | 1,400             | 1,390 (weaken)                               |
| P=S                   | 778                             | 778                | 778               | 778               | 778                   | 778               | 778  |
|                       | ~561                            | ~561               | ~561              | ~561              | ~561                  | ~561              | ~561   |

Table 2  
Biosorption capacity of Cu(II) onto the chemically treated MTB

| MTB (%) | Modified MTB (%) |             |   |
|---------|------------------|-------------|---|
|         | -COOH blocked    | -OH blocked | -PO <sub>3</sub> H <sub>2</sub> blocked |
| 98.4    | 59.7             | 82.8        | 90.2                                    |

Table 3  
Regression results from the potentiometric titration

|                                 | <i>pK<sub>a</sub></i> | <i>N</i> (mmol/g) | <i>pK<sub>a</sub></i> in literatures | Number of groups (nm <sup>-2</sup> ) |
|---------------------------------|-----------------------|-------------------|--------------------------------------|--------------------------------------|
| -COOH                           | 3.4664                | 0.3325            | 1.7–4.7 [47, 48]                     | 5                                    |
| -PO <sub>3</sub> H <sub>2</sub> | 6.2095                | 0.5133            | 6.1–6.8 [49]                         | 8                                    |
| -OH                             | 9.6162                | 0.6410            | 9.5–13 [50]                          | 10                                   |

The number of groups was calculated from Table 3 [53]:  $1 \times 10^{13}$  cells per liter were found when the biomass was 2.5 g/l [54], i.e.  $4 \times 10^{12}$  cells per gram of biomass. The number of -COOH groups per gram of biomass was  $N_i \times N_A = 0.3325 \times 10^{-3} \times 6.023 \times 10^{23} = 2.003 \times 10^{20}$ , in which  $N_A$  is Avogadro's constant. Thus, the number of -COOH groups per cell was  $2.005 \times 10^{20} / 4 \times 10^{12} = 5.007 \times 10^7$ . The MTB was usually a short rod cell that had a diameter of approximately 1.0 μm and a length of 3.0 μm in length [29], i.e. its surface area was  $9.424 \times 10^6$  nm<sup>2</sup>. Therefore, the number of -COOH groups per square nanometer was  $5.012 \times 10^7 / 9.424 \times 10^6 \approx 5$ . The number of -PO<sub>3</sub>H<sub>2</sub> and -OH groups was calculated in the same manner as shown in Table 3.

According to the above experiments, the three groups, i.e. -COOH, -OH, and -PO<sub>3</sub>H<sub>2</sub>, were considered

to be the functional groups in the MTB adsorption process. Therefore, the structure of an MTB molecule could be presented as shown in Fig. 2. The charge parameters of the groups using CHARMM force field are listed in Table 4. Atoms of carbon skeleton were adjusted in charge to balance the net charge of the whole MTB molecule.

### 3.2. Gibbs free energy change for adsorption

As an example of the simulation, Cu(II) was first calculated in the simulated system. Fig. 3 shows the total energy of the simulated system and the average atomic root-mean-square displacements (RMSDs) of Cu(II) during the 20 ps of minimization and 4 ns of relaxation. Both the energy and the RMSD of the ion maintained stable states in the second half of the

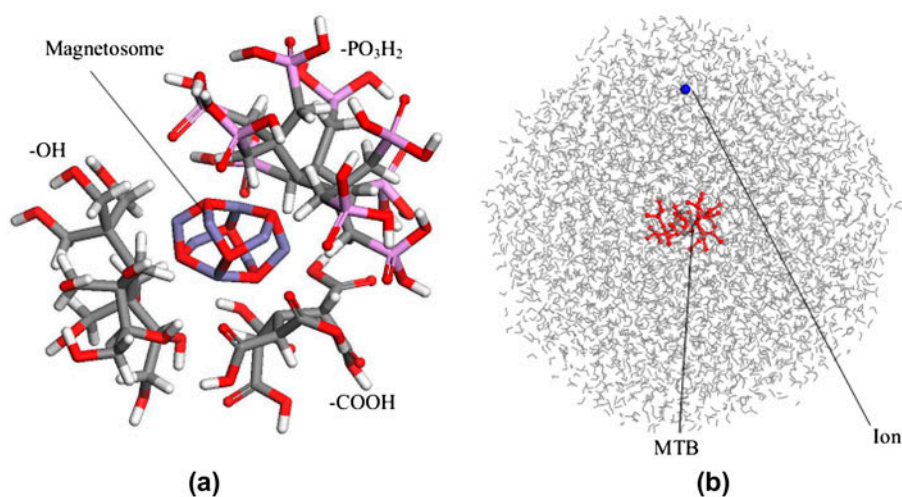


Fig. 2. Structure of the MTB molecule and the simulated system (a) MTB molecule and (b) Spherical simulation system.

Table 4  
Charge parameters of the groups

| Atom | Atom charge | Group                  | Group net charge |
|------|-------------|------------------------|------------------|
| C    | 0.75        | -CO(1)O(2)H            | 0.03             |
| O(1) | -0.55       |                        |                  |
| O(2) | -0.61       |                        |                  |
| H    | 0.44        |                        |                  |
| O    | -0.66       | -OH                    | -0.23            |
| H    | 0.43        |                        |                  |
| P    | 1.5         | -PO(1)O(2)H(2)O(2)H(2) | 0.46             |
| O(1) | -0.64       |                        |                  |
| O(2) | -0.63       |                        |                  |
| H(2) | 0.43        |                        |                  |

relaxation, which indicates that an energy equilibrium was reached. Fig. 3 also indicates that the Cu(II) ended at a distance ( $\zeta$ ) of approximately 20 Å from the center of the MTB molecule. In this simulation, the MTB had a radius of 7 Å; therefore, Cu(II) found to be 13 Å from the surface of the MTB, which was exactly the cutoff length in this simulation. To be adsorbed, Cu(II) had to be pushed to the space within the capture range of the surface groups on the MTB and then continue to move toward the MTB, thus reducing its distance to the MTB center ( $\zeta$ ) to less than 20 Å.

Using the SMD method, the Cu(II) forcibly pushed toward and pulled away from the MTB. The force applied to the Cu(II) and the  $\zeta$  between Cu(II) and the MTB in the SMD process are shown in Fig. 4. The pushed Cu(II) exhibited faster movement before it

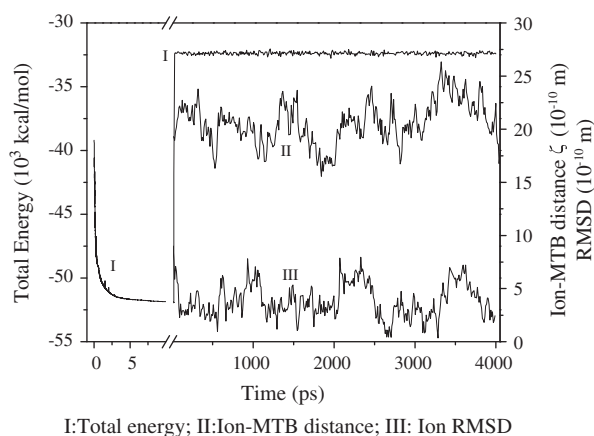


Fig. 3. Energy minimization and equilibrium of the simulated system.

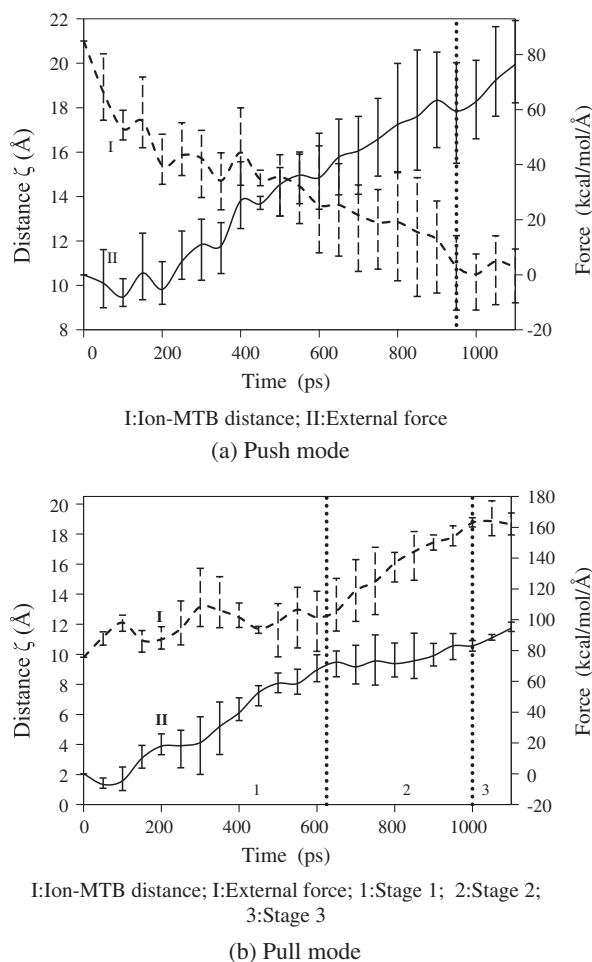


Fig. 4. Force and distance profiles delineating the ionic diffusion.

reached a distance of 12 Å from MTB center and subsequently showed slower movement with a change in the external force. However, a slightly higher force was required to push the Cu(II) across the 15 Å boundary away from the MTB center; otherwise, the Cu(II) could not be spontaneously captured by the MTB, which indicates that the Cu(II) encountered a repulsive force on approaching the MTB.

From Fig. 4, it can be deduced that a repulsive force obstructed the combination of Cu(II) with the MTB as the Cu(II) left its equilibrium position of 20 Å from the MTB center. Once it entered the space less than 12 Å from the MTB center, the Cu(II) position was slightly changed, which corroborated the adsorption of Cu(II) onto the MTB surface. The distance of 5 Å between Cu(II) and the MTB surface groups was generally considered an adsorbent–adsorbate distance for physical adsorption [55].

The ionic reverse movement was also studied as shown in Fig. 4(b), i.e. the Cu(II) was pulled from the MTB surface. The process of moving the Cu(II) was divided into three stages based on force and displacement. The first stage represented ionic motion within a range of 12 Å around the center of the MTB, i.e. less than 5 Å from the MTB surface. Obviously, in this region the external force on Cu(II) was increasing to overcome the attraction of the MTB so that the Cu(II) could escape, which reveals the interaction between the MTB and Cu(II) to be a type of attractive force. During the second stage, Cu(II) moved from 12 to 20 Å away from the MTB center. In this stage, the force applied to the Cu(II) was almost constant, but the distance between the Cu(II) and MTB center was increasing, which indicates the desorption of the Cu(II) with the application of an external force. The third stage occurred when the Cu(II) moved out of the space 20 Å away from the MTB center. In the third stage, Cu(II) displacement slowed despite the gradually increasing external force. At distances greater than 20 Å away from the MTB center (i.e. more than the 12 Å cutoff length from the MTB surface groups), no interaction occurred between the MTB and the Cu(II) in the calculation. The slowing of Cu(II) displacement without any MTB interaction in the third stage also revealed that the interaction between MTB and Cu(II) in the second stage involves a repulsive force. As a result, it can be deduced that the dividing line between attraction and repulsion of Cu(II) by the MTB was located at the 5 Å boundary from the MTB surface groups.

Figs. 3 and 4 indicate that the equilibrium positions for the free diffusion and forced adsorption of Cu(II) were 20 and 12 Å from the MTB center, respectively. Therefore, the differences in free energy of the Cu(II) at these two positions were compared during the forced movement process as shown in Fig. 5, which demonstrates an approximately 4.56 kcal/mol drop in the free energy when the Cu(II) left its equilibrium position of free diffusion to be adsorbed.

Experimentally, the standard Gibbs free energy in the adsorption process was calculated using the following equation [56]:

$$\Delta G^\circ = -RT \ln b \quad (1)$$

in which  $b$  (L/mol) is the equilibrium constant obtained from  $b$  (L/mg) of the Langmuir model,  $T$  is the temperature (in K), and  $R$  (8.314 J/mol K) is the gas universal constant. Using this method, the free energy changes for Cu(II) and other ions were calculated based on the experimental results in the literature [12,13] and then compared with the values

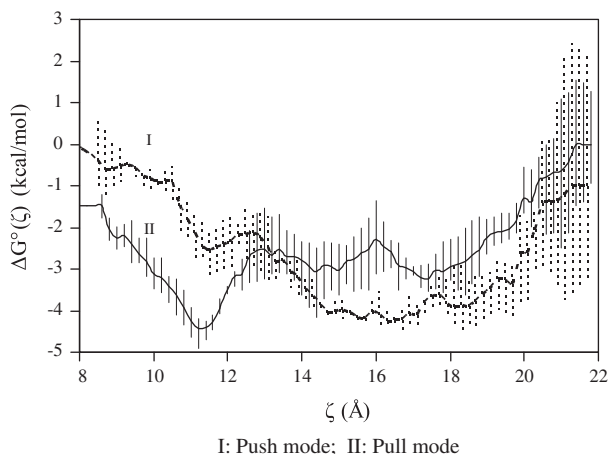


Fig. 5. Free energy profiles delineating the ionic diffusion.

obtained from this simulation as shown in Table 5. The simulated free energies were in accordance with the experimental values. Because all energy changes were less than 9.56 kcal/mol (40 kJ/mol), physical adsorption was proposed as a possible mechanism [57], which was confirmed because the temperature had little effect on the adsorption capacity of MTB for ions [12,13].

Generally, as the free energy decreased, adsorbates were more easily captured by the adsorbent during the adsorption process. According to this principle, the order in which the ions were adsorbed in the multi-component system should be Au(III) > Ag(I) > Ni(II) > Cu(II), which was confirmed by the literature [12,13].

### 3.3. Ionic diffusion with different charges and masses

A virtual observation of the free energy changes during adsorption are shown in Fig. 6. Although this figure does not have physical implications, some useful information can be obtained. Fig. 6 shows that the magnitude of an ion's free energy drop increased as

its charge and mass increased; as a result, the ion was more likely to be adsorbed. This pattern was found to be in accordance with the experimental study [12,13], in which the order of adsorption priority was Au(III) > Cu(II) and Ag(I) > Cu(II). Based on these findings, one could speculate that light metal ions such as Na<sup>+</sup> and Mg<sup>2+</sup> will not adsorb, which was also consistent with the experimental results.

The phenomenon in Fig. 6 can be explained, to a certain extent, by Fig. 7. When the mass of an ion was small, a free energy change was observed at a distance of 16 Å from the adsorbent center. However, ions with a larger mass caused a free energy drop at a distance of about 11 Å from the adsorbent center. In addition, the free energy drop occurring from the larger mass ion was greater than free energy drop caused by the smaller mass ion. These findings suggest that ions with small mass are not completely attracted to the adsorbent, but instead encounter more repulsive forces during the adsorption process. Therefore, we hypothesized that an ion with a small mass would be more inclined toward free and disordered thermal diffusion and thus could not quickly adsorb, because of the weak inertia arising from its small mass. In comparison, only ions with large masses can be steadily pushed onto the adsorbent by the virtual external force, resulting in adsorption.

Another piece of information obtained from Fig. 6 was that an ion having a higher valence was more likely to adsorb than an ion having a lower valence, given equal conditions. It is known that the ionic valence directly determines the size of the Coulomb force; therefore, the above phenomenon indicates that electrostatic interaction is one of the aspects promoting the adsorption. We verified this inference by performing a univariate analysis, whereby only van der Waals or Coulomb forces were incorporated. Setting the charge and  $\epsilon$  to zero, we separately simulated adsorption processes to isolate the van der Waals and Coulomb forces, respectively. The ionic free energy change during adsorption is shown in Fig. 8. From this figure, it can be seen that the free energy did not decrease,

Table 5  
Gibbs free energy for the adsorption of the cations onto the MTB

|         |          | Experimental results |             |                             | Simulation work             |
|---------|----------|----------------------|-------------|-----------------------------|-----------------------------|
|         |          | $b$ (L/mg)           | $b$ (L/mol) | $\Delta G^\circ$ (kcal/mol) | $\Delta G^\circ$ (kcal/mol) |
| Cu(II)  | [13]     | 0.0215               | 1,366.24    | -4.28                       | -4.56                       |
|         | [12]     | 0.1605               | 10,199.1    | -5.47                       |                             |
| Au(III) | [12]     | 0.978                | 192,633     | -7.2                        | -7.06                       |
| Ag(I)   | [13]     | 1.7055               | 183,969     | -7.18                       | -5.9                        |
| Ni(II)  | Measured | 0.146                | 8,569.24    | -5.36                       | -5.17                       |

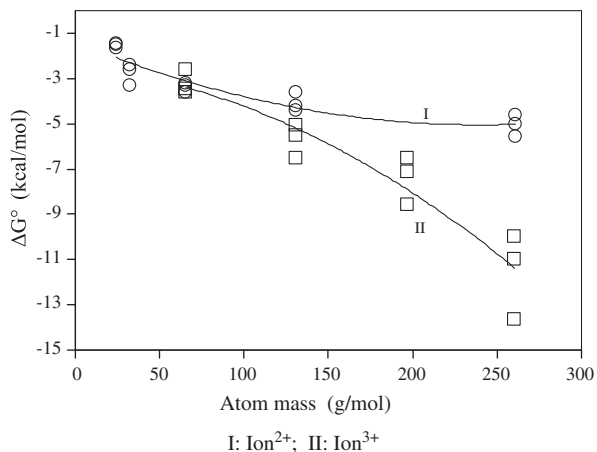


Fig. 6. Free energy change of ions with different atom masses.

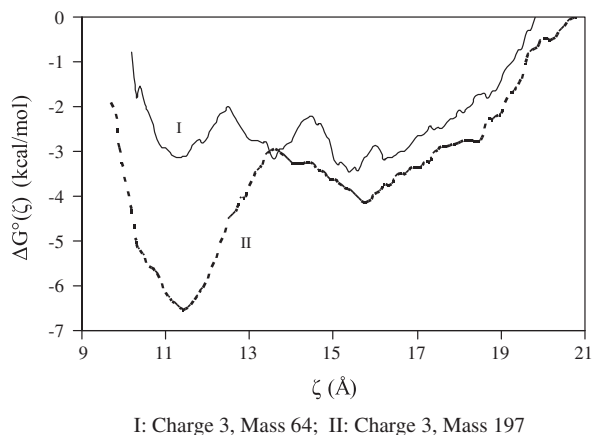


Fig. 7. Free energy profiles delineating the distribution of virtual ions.

but instead continued to rise as an ion approached the adsorbent driven by the isolated van der Waals force. The ionic free energy decreased only when the Coulomb force was present in the simulation, revealing that the electrostatic attraction was a major factor promoting adsorption, while the van der Waals force prevented adsorption. These findings are consistent with the literature [24].

The van der Waals force exists not only between ions and the adsorbent but also between ions and the surrounding water molecules. Therefore, compared with the Coulomb force, the van der Waals force has a broader impact, meaning that ion adsorption was influenced by the van der Waals force. Relatively speaking, the greater the ion's mass, which means that the van der Waals force will have a greater influence

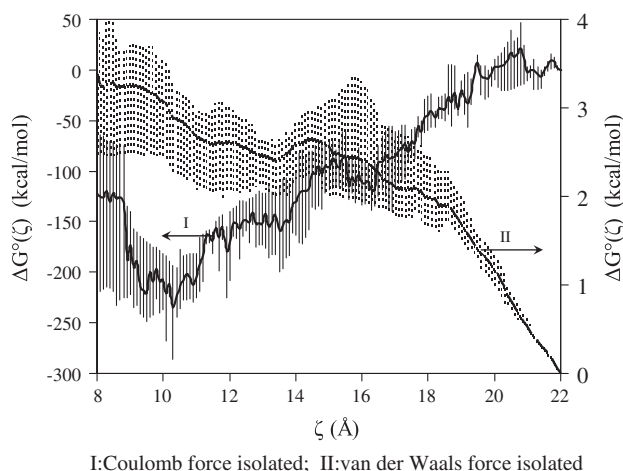


Fig. 8. Free energy profiles delineating the ionic diffusion under virtual forces.

on the ion. In this case, the surrounding water molecules and the ion's own inertia limit the disordered displacement of the ion, allowing it to move steadily toward the adsorbent under the action of the external energy. The simulation showing the free diffusion of ions clearly explained this phenomenon. The external energy mentioned above was not specifically simulated in this work. From a biological viewpoint, the bacterial (adsorbent) metabolism provided the energy source for the adsorption of metal ions.

### 3.4. Ionic diffusion and adsorption selectivity

To study the role of a single group on the adsorption of an ion, the simulation was performed with the same configuration as shown in Fig. 2(b), but only one type of functional group was used. The ionic diffusion and free energy change were investigated in the simulation process. The trajectory probability was used to characterize the tendency of ions to move toward the functional groups as shown in Fig. 9. The probability densities of the ions trajectory indicated that the distance between the ions and the  $-\text{COOH}$  was lowest in a state of equilibrium, which indicates that among the studied groups,  $-\text{COOH}$  had the highest attraction to ions. The free energy change shown in Table 6 simultaneously revealed that the energy drop increased more when an ion (virtual  $\text{Cu(II)}$ ) approached  $-\text{COOH}$  relative to other groups. In conclusion, Fig. 9 demonstrates that the likelihood of ion capture was highest for  $-\text{COOH}$ , followed by  $-\text{OH}$ ,  $-\text{PO}_3\text{H}_2$ , and  $\text{Fe}_3\text{O}_4$  in that order. Combined with the chemical modification experiments shown in Table 5, it can be concluded that  $-\text{COOH}$  was the primary group for adsorption.

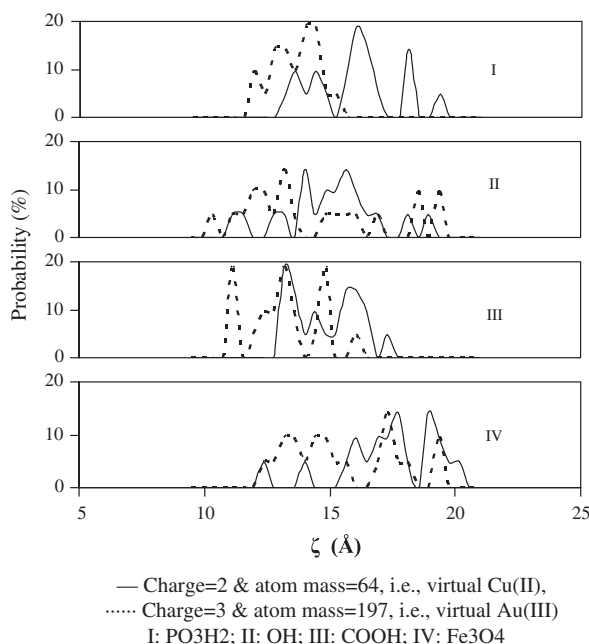


Fig. 9. Probability distributions in the ionic diffusion.

Several examples of Cu(II) adsorption on  $-\text{COOH}$ -terminated surfaces [58] have been reported to arise from specific copper surface interactions and the formation of Cu(II)-carboxylate complexes. In this simulation, the combination of Cu(II) and  $-\text{COOH}$  proved to be stable with regard to the energy change and ionic diffusion.

To investigate the effect of the features of the ions on the diffusion process, other ions were introduced into the system to provide contrast with the virtual Cu(II). Therefore, an ion with larger charge and mass (virtual Au(III)) was added into the groups system, and a dynamics simulation was performed. The trajectory probability distributions of the additional ion are also shown in Fig. 9. The two ions exhibited similar diffusion behavior. The  $-\text{COOH}$  group was the most able to capture ions, followed by  $-\text{OH}$  and  $-\text{PO}_3\text{H}_2$ . However, differences remained in the abilities of the groups to capture the two ions. For  $-\text{PO}_3\text{H}_2$ , the trajectory ranges of Au(III) and Cu(II) overlap a little, which

indicates that the ability of  $-\text{PO}_3\text{H}_2$  to capture Au(III) and Cu(II) could be easily distinguished. The trajectory range of Au(III) was closer to  $-\text{PO}_3\text{H}_2$  than that of Cu(II), and the maximum probability for Au(III) was higher than that for Cu(II), both of which imply that Au(III) was more easily captured by this group than Cu(II). The Cu(II) was thus more likely to drift away from the  $-\text{PO}_3\text{H}_2$ . For  $-\text{OH}$ , the trajectory ranges of Au(III) and Cu(II) partially overlapped, which indicates that the ability of  $-\text{OH}$  to capture Au(III) or Cu(II) was apparently indistinguishable. The trajectory ranges of Au(III) and Cu(II) also partially overlapped  $-\text{COOH}$ . The site of maximum Au(III) probability was closer to  $-\text{COOH}$  than that of Cu(II), which indicates a higher capture tendency of  $-\text{COOH}$  for Au(III). For  $\text{Fe}_3\text{O}_4$ , the trajectory ranges of Au(III) and Cu(II) overlapped almost completely, and the locations of maximum Au(III) and Cu(II) probability were almost the same; because  $\text{Fe}_3\text{O}_4$  has a neutral charge (and thus exerts the same electric force), it had the same ability to capture Au(III) and Cu(II).

Fig. 9 indicates that  $-\text{PO}_3\text{H}_2$  and  $-\text{COOH}$  both preferentially captured the virtual Au(III), whereas  $-\text{OH}$  and  $\text{Fe}_3\text{O}_4$  remained neutral during the capture process. Additional studies were performed to determine how a combination of these functional groups would influence the adsorption selectivity of ions. Thus, the MTB molecule in Fig. 2 was placed into a binary solution of virtual Au(III) and Cu(II). A molecular dynamics simulation was run to compare the trajectory probabilities of ions as shown in Fig. 10. The shortest distance between Au(III) and the MTB was  $15 \text{ \AA}$ , whereas that for the Cu(II) remained  $17 \text{ \AA}$ . Thus, from the ion diffusion angles, it could be deduced that Au(III) was more likely than the Cu(II) to adsorb onto the MTB.

Because the ions were adsorbed in the same environments, the mechanism by which the Cu(II) lost adsorption priority likely depended on the nature of the ion itself. In general, the electric force imposed on an ion is proportional to the charge carried by the ion, and the resulting acceleration is inversely proportional to the ion mass. Thus, the movement of the ion depends on its charge–mass ratio. The charge on an electron is  $1.602 \times 10^{-19} \text{ C}$ ; thus, the charge–mass ratio for Cu(II) is as follows:

$$\frac{q}{m} = \frac{1.602 \times 10^{-19} \text{ C} \times 2}{63.546 \times 10^{-3} \text{ kg mol}^{-1} / 6.023 \times 10^{23} \text{ mol}^{-1}} = 3.0368 \times 10^6 \text{ C/kg}$$

in which  $q$  and  $m$  are the charge and the mass of the ion, respectively.

Table 6

Gibbs free energy for the adsorption of the cations onto the functional groups of MTB

| Gibbs free energy change (kcal/mol) |              |                          |                         |
|-------------------------------------|--------------|--------------------------|-------------------------|
| $-\text{COOH}$                      | $-\text{OH}$ | $-\text{PO}_3\text{H}_2$ | $\text{Fe}_3\text{O}_4$ |
| 2.75                                | 2.5          | 2.5                      | 2.07                    |

Note: Charge = 2 & atom mass = 64, virtual Cu(II).

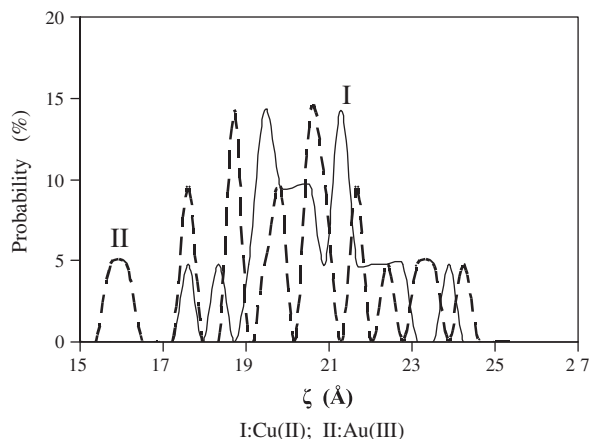


Fig. 10. Probability distribution in the ionic diffusion attracted by the MTB.

The charge–mass ratio for Au(III) is as follows:

$$\frac{q}{m} = \frac{1.602 \times 10^{-19} \text{ C} \times 3}{196.967 \times 10^{-3} \text{ kg mol}^{-1} / 6.023 \times 10^{23} \text{ mol}^{-1}} = 1.4696 \times 10^6 \text{ C/kg}$$

Therefore, the charge–mass ratio of Cu(II) is higher than that of Au(III), which results in a higher activity of Cu(II) during diffusion. However, Figs. 4 and 8 demonstrate that the non-bonded forces in the diffusion of the ions toward the MTB act as a repulsive force. Therefore, an ion with a higher charge–mass ratio has more difficulty in moving toward the MTB, which could justify the low priority of Cu(II) adsorption from the Cu(II)–Au(III) solution [12] and in similar multi-cation systems such as Cu(II)–Ag(I) solutions [13].

#### 4. Conclusions

The physical forces generated by bacterial surface groups were found to influence the biosorption using molecular dynamics simulation. A model of the MTB module was built based on associations with  $-\text{PO}_3\text{H}_2$ ,  $-\text{OH}$ ,  $-\text{COOH}$ , and  $\text{Fe}_3\text{O}_4$ . The  $-\text{PO}_3\text{H}_2$ ,  $-\text{OH}$ , and  $-\text{COOH}$  groups exhibited concentrations of 8, 10, and 5 / $\text{nm}^2$  on the MTB surface, respectively. In this simulation, the ions forcibly diffused from 20 Å to 12 Å from the MTB center, after which physical adsorption was believed to occur. A repulsive force had to be overcome when an ion was adsorbed onto the MTB. According to the energy calculations, the order of ion competitive adsorption in the multi-component solutions was  $\text{Au(III)} > \text{Ag(I)} > \text{Ni(II)} > \text{Cu(II)}$ . The

electrostatic attraction between ions and the adsorbent promotes adsorption, while the van der Waals force hinders adsorption. Moreover, the van der Waals force is one of the key factors in determining an ion's tendency toward adsorption. Based on the trajectory probability density, the functional groups were found to differ in their ability to attract ions. The  $-\text{PO}_3\text{H}_2$  and  $-\text{COOH}$  groups contributed to the adsorption selectivity during the entire adsorption process in the multi-component solutions.

#### Acknowledgments

This paper presented at the International DWT Academic Seminar, 2013 Qingdao International Conference on Desalination and Water Reuse, June 25–28, 2013, Qingdao, China. This work was financially supported by National Natural Science Foundation of China (51104097, 20906053), the Research Projects of Shanxi Province (2012021010-2, 20120313014-1), and the Program of International Science and Technology Cooperation (2012DFA91500).

#### References

- [1] M.T. Sulak, H.C. Yatmaz, Removal of textile dyes from aqueous solutions with eco-friendly biosorbent, *Desalin. Water Treat.* 37 (2012) 169–177.
- [2] L.D.T. Prola, E. Acayanka, E.C. Lima, C. Bestetti, W.O. Santos, F.A. Pavan, S.L.P. Dias, C.R.T. Tarley, Application of aqai stalks as biosorbent for the removal of Evans Blue and Vilmafix Red RR-2B dyes from aqueous solutions, *Desalin. Water Treat.* 51 (2013) 4582–4592.
- [3] H.P. Song, X.G. Li, J.S. Sun, S.M. Xu, X. Han, Application of a magnetotactic bacterium, *Stenotrophomonas* sp. to the removal of Au(III) from contaminated wastewater with a magnetic separator, *Chemosphere* 72 (2008) 616–621.
- [4] Y. Ji, H. Gao, J. Sun, F. Cai, Experimental probation on the binding kinetics and thermodynamics of Au(III) onto *Bacillus subtilis*, *Chem. Eng. J.* 172 (2011) 122–128.
- [5] S.L. Simmons, D.A. Bazylinski, K.J. Edwards, South-seeking magnetotactic bacteria in the Northern Hemisphere, *Science* 311 (2006) 371–374.
- [6] D.A. Bazylinski, S. Schübbe, Controlled biomineralization by and application of magnetotactic bacteria, *Adv. Appl. Microbiol.* 62 (2007) 21–62.
- [7] J. Xie, K. Chen, X. Chen, Production, modification and bio-applications of magnetic nanoparticles gestated by magnetotactic bacteria, *Nano Res.* 2 (2009) 261–278.
- [8] F. Cai, J. Li, J. Sun, Y. Ji, Biosynthesis of gold nanoparticles by biosorption using *Magnetospirillum gryphiswaldense* MSR-1, *Chem. Eng. J.* 175 (2011) 70–75.
- [9] T.M. Petrova, L. Fachikov, J. Hristov, The magnetite as adsorbent for some hazardous species from aqueous solutions: A review, *Int. Rev. Chem. Eng.* 3 (2011) 134–152.

- [10] M.S. Marius, P.A.B. James, A.S. Bahaj, D.J. Smallman, Development of a highly magnetic iron sulphide for metal uptake and magnetic separation, *J. Magn. Magn. Mater.* 293 (2005) 567–571.
- [11] A.S. Bahaj, P.A.B. James, F.D. Moeschler, Low magnetic-field separation system for metal-loaded magnetotactic bacteria, *J. Magn. Magn. Mater.* 177–181 (1998) 1453–1454.
- [12] H.P. Song, X.G. Li, J.S. Sun, Equilibrium and kinetic modelling of biosorption of Au(III) and Cu(II) on magnetotactic bacteria (MTB), *Chin. J. Chem. Eng.* 15 (2007) 847–854.
- [13] H.P. Song, X.G. Li, H.G. Cheng, F.Q. Cheng, Theoretical and experimental study of Au(III)-containing wastewater treatment using magnetotactic bacteria, *Desalin. Water Treat.* 51(19–21) (2013) 3864–3870.
- [14] Y.H. Wang, H. Gao, J.S. Sun, J. Li, Y.X. Su, Y.L. Ji, C.M. Gong, Selective reinforced competitive biosorption of Ag(I) and Cu(II) on *Magnetospirillum gryphiswaldense*, *Desalination* 270 (2011) 258–263.
- [15] A.H. Sulaymon, D.W. Abbood, A.H. Ali, A comparative adsorption/biosorption for the removal of phenol and lead onto granular activated carbon and dried anaerobic sludge, *Desalin. Water Treat.* 51 (2013) 2055–2067.
- [16] M. Calero, G. Blázquez, E. Dionisio-Ruiz, A. Ronda, M.A. Martín-Lara, Evaluation of biosorption of copper ions onto pinion shell, *Desalin. Water Treat.* 51 (2013) 2411–2422.
- [17] L. Zhang, Y. Sun, Molecular simulation of adsorption and its implications to protein chromatography: A review, *Biochem. Eng. J.* 48 (2010) 408–415.
- [18] H. Roohi, E. Zahiri, Thermodynamic and topological investigation of the interaction between methimazole and  $M^{2+}$  ( $Na^+$ ,  $Li^+$ ,  $Ca^{2+}$  and  $Mg^{2+}$ ), *Comput. Theor. Chem.* 984 (2012) 113–118.
- [19] C.H. Hou, W.J. Shi, F.D. Ren, Y. Wang, J.Y. Wang, A B3LYP and MP2(full) theoretical investigation into explosive sensitivity upon the formation of the molecule–cation interaction between the nitro group of  $RNO_2$  ( $R = -CH_3, -NH_2, -OCH_3$ ) and  $Na^+$ ,  $Mg^{2+}$  or  $Al^{3+}$ , *Comput. Theor. Chem.* 991 (2012) 107–115.
- [20] B. Jagoda-Cwiklik, L. Cwiklik, Coarse grain simulations of the influence of adsorbate–adsorbate interactions on adsorption and diffusion of n-butane in silicalite-1, *Chem. Phys. Lett.* 445 (2007) 42–46.
- [21] H. Yang, Z.Y. Lu, Z.S. Li, C.C. Sun, A molecular-dynamics simulation study of diffusion of a single model carbonic chain on a graphite (001) surface, *J. Mol. Model.* 12 (2006) 432–435.
- [22] N. Jalili, K. Laxminarayana, A review of atomic force microscopy imaging systems: Application to molecular metrology and biological sciences, *Mechatronics* 14 (2004) 907–945.
- [23] L.O. Atovmyan, S.V. Konovalikhin, The effect of non-bonded interactions on the electronic structure of anions in XSCN crystals ( $X = NH_4, Na$ ), *J. Mol. Struct.* 412 (1997) 69–74.
- [24] D.E.B. Gomes, R.D. Lins, P.G. Pascutti, C. Lei, T.A. Soares, The role of non-bonded interactions in the conformational dynamics of organophosphorous hydrolase adsorbed onto functionalized mesoporous silica surfaces, *J. Phys. Chem. B.* 114 (2010) 531–540.
- [25] M. Patra, M. Karttunen, M.T. Hyvönen, E. Falck, P. Lindqvist, I. Vattulainen, Molecular dynamics simulations of lipid bilayers: Major artifacts due to truncating electrostatic interactions, *Biophys. J.* 84 (2003) 3636–3645.
- [26] T. Düren, Y.-S. Bae, R.Q. Snurr, Using molecular simulation to characterise metal–organic frameworks for adsorption applications, *Chem. Soc. Rev.* 38 (2009) 1237–1247.
- [27] R.D. Groot, Electrostatic interactions in dissipative particle dynamics—Simulation of polyelectrolytes and anionic surfactants, *J. Chem. Phys.* 118 (2003) 11265–11278.
- [28] E. Fourest, B. Volesky, Contribution of sulfonate groups and alginate to of *Sargssum fluitans*, *Crit. Rev. Environ. Sci. Technol.* 30 (1996) 277–282.
- [29] H.P. Song, Selective Biosorption Behavior of Precious Metal Ions on Magnetotactic Bacteria and Gold recovery from Gold(III) Contained Solution, PhD Thesis, Tianjin University, China, 2008 (In Chinese).
- [30] J.C. Phillips, R. Braun, W. Wang, J. Gumbart, E. Tajkhorshid, E. Villa, C. Chipot, R.D. Skeel, L. Kalé, K. Schulten, Scalable molecular dynamics with NAMD, *J. Comput. Chem.* 26 (2005) 1781–1802.
- [31] W. Humphrey, A. Dalke, K. Schulten, VMD: Visual molecular dynamics, *J. Mol. Graph.* 14 (1996) 33–38.
- [32] S.D. Hong, M.Y. Ha, S. Balachandar, Static and dynamic contact angles of water droplet on a solid surface using molecular dynamics simulation, *J. Colloid Interface Sci.* 339 (2009) 187–195.
- [33] C. Rovira, Role of the His64 residue on the properties of the Fe–CO and Fe–O<sub>2</sub> bonds in myoglobin: A CHARMM/DFT study, *J. Mol. Struct.-Theochem.* 632 (2003) 309–321.
- [34] H.E. Alper, P. Politzer, Chapter 17 molecular dynamics simulation of copper using CHARMM: Methodological considerations and initial results, *Theor. Comput. Chem.* 7 (1999) 703–736.
- [35] A.V. Akimov, A.V. Nemukhin, A.A. Moskovsky, A.B. Kolomeisky, J.M. Tour, Molecular dynamics of surface-moving thermally driven nanocars, *J. Chem. Theory Comput.* 4 (2008) 652–656.
- [36] R. Braun, M. Sarikaya, K. Schulten, Genetically engineered gold-binding polypeptides: Structure prediction and molecular dynamics, *J. Biomater. Sci. Polym. Ed.* 13 (2002) 747–757.
- [37] T.K. Kundu, K. Rao, S.C. Parker, Atomistic simulation studies of magnetite surface structures and adsorption behavior in the presence of molecular and dissociated water and formic acid, *J. Colloid Interface Sci.* 295 (2006) 364–373.
- [38] S.Á. Kovács, C.S. Lo, Electronic structure and charge ordering in magnetite: implications for the Fe<sub>3</sub>O<sub>4</sub>(001)-water interface, *Mol. Simul.* 36(15) (2010) 1289–1296.
- [39] A.K. Rappe, C.J. Casewit, K.S. Colwell, W.A. Goddard, W.M. Skiff, UFF, a full periodic table force field for molecular mechanics and molecular dynamics simulations, *J. Am. Chem. Soc.* 114 (1992) 10024–10035.
- [40] S. Parthasarathy, F. Long, Y. Miller, Y. Xiao, D. McElheny, K. Thurber, B. Ma, R. Nussinov, Y. Ishii, Molecular-level examination of Cu<sup>2+</sup> binding structure for amyloid fibrils of 40-residue alzheimers  $\beta$  by solid-state nmr spectroscopy, *J. Am. Chem. Soc.* 133 (2011) 3390–3400.

- [41] L. Miao, J.M. Seminario, Molecular dynamics simulations of the vibrational signature transfer from a glycine peptide chain to nanosized gold clusters, *J. Phys. Chem. C* 111 (2007) 8366–8371.
- [42] G. Gamez, J.L. Gardea-Torresdey, K.J. Tiemann, J. Parsons, K. Dokken, M.J. Yacaman, Recovery of gold(III) from multi-elemental solutions by alfalfa biomass, *Adv. Environ. Res.* 7 (2003) 563–571.
- [43] C.E. Dogan, K. Turhan, G. Akcin, A. Aslan, Biosorption of Au (III) and Cu (II) from aqueous solution by a non-living *Cetraria Islandica* (L.) Ach, *Ann. Chim.* 96 (2006) 229–236.
- [44] L.G. Benning, V.R. Phoenix, N. Yee, M.J. Tobin, Molecular characterization of cyanobacterial silicification using synchrotron infrared micro-spectroscopy, *Geochimica et Cosmochimica Acta* 68 (2004) 729–741.
- [45] G. Naja, C. Mustin, B. Volesky, J. Berthelin, A high resolution titrator: A new approach to studying binding sites of microbial biosorbents, *Water Res.* 39 (2005) 579–588.
- [46] P. Mukherjee, S. Senapati, D. Mandal, A. Ahmad, M.I. Khan, R. Kumar, M. Sastry, Extracellular synthesis of gold nanoparticles by the fungus *Fusarium oxysporum*, *Chembiochem* 3(5) (2002) 461–463.
- [47] B. Volesky, Sorption and Biosorption, Quebec, BV-Sorbex Inc., St. Lambert, 2003, p. 41.
- [48] N. Yee, L.G. Benning, V.R. Phoenix, F. Grant Ferris, Characterization of metal-cyanobacteria sorption reactions: A combined macroscopic and infrared spectroscopic investigation, *Environ. Sci. Tec.* 38 (2004) 775–782.
- [49] T.J. Beveridge, R.G.E. Murray, Sites of metal deposition in the cell wall of *Bacillus subtilis*, *J. Bacteriol.* 141 (1980) 876–887.
- [50] J.Y. Wang, S.G. Zhu, C.F. Xu, *Biological Chemistry*, third ed., Higher Education Press, Beijing, 2002, p. 131 (In Chinese).
- [51] H. Seki, A. Suzuki, S.I. Mitsueda, Biosorption of heavy metal ions on *Rhodobacter sphaeroides* and *Alcaligenes eutr. phush16*, *J. Colloid Interf. Sci.* 197 (1994) 185–190.
- [52] Y.S. Yun, B. Volesky, Modeling of lithium interference in cadmium biosorption, *Environ. Sci. Technol.* 37 (2003) 3601–3608.
- [53] H.P. Song, H.G. Cheng, F.Q. Cheng, Simulation on biosorption of Ni<sup>2+</sup> by magnetotactic microorganism in aqueous solution, *Ion Exch. Ads.* 27 (2011) 392–399 (In Chinese).
- [54] J.B. Fein, C.J. Daughney, N. Yee, T.A. Davis, A chemical equilibrium model for metal adsorption onto bacterial surface, *Geochim. Cosmochim. Acta* 61 (1997) 3319–3328.
- [55] X.L. Dong, Q. Wang, T. Wu, H.H. Pan, Understanding adsorption-desorption dynamics of BMP-2 on hydroxyapatite (001) surface, *Biophysical J.* 93 (2007) 750–759.
- [56] K.S. Tong, M. Jain, Kassim, A. Azraa, Adsorption of copper ion from its aqueous solution by a novel biosorbent *Uncaria gambir*: Equilibrium, kinetics, and thermodynamic studies, *Chem. Eng. J.* 170 (2011) 145–153.
- [57] M. Horsfall Jr, A.I. Spiff, A.A. Abia, Studies on the influence of mercapt oacetic acid (MAA) modification of cassava (*Manihot sculenta* Cranz) waste biomass on the adsorption of Cu<sup>2+</sup> and Cd<sup>2+</sup> from aqueous solution, *Bull. Korean Chem. Soc.* 25 (2004) 969–976.
- [58] P. Lu, Z. Shi, A.V. Walker, Selective electroless deposition of copper on organic thin films with improved morphology, *Langmuir* 27 (2011) 13022–13028.